Published in final edited form as:
J Vis. ; 7(14): 20.1–2011. doi:10.1167/7.14.20.

Thalamic filtering of retinal spike trains by postsynaptic summation

Matteo Carandini,
Smith-Kettlewell Eye Research Institute, San Francisco

Jonathan C. Horton, and
Beckman Vision Center, University of California, San Francisco

Lawrence C. Sincich
Beckman Vision Center, University of California, San Francisco

Matteo Carandini: matteo@ski.org; Jonathan C. Horton: hortonj@vision.ucsf.edu; Lawrence C. Sincich: sincichl@vision.ucsf.edu

Abstract

At many synapses in the central nervous system, spikes within high-frequency trains have a better chance of driving the postsynaptic neuron than spikes occurring in isolation. We asked what mechanism accounts for this selectivity at the retinogeniculate synapse. The amplitude of synaptic potentials was remarkably constant, ruling out a major role for presynaptic mechanisms such as synaptic facilitation. Instead, geniculate spike trains could be predicted from retinal spike trains on the basis of postsynaptic summation. This simple form of integration explains the response differences between a geniculate neuron and its main retinal driver, and thereby determines the flow of visual information to cortex.

Introduction

Most neurons communicate through rapid sequences of action potentials, but the transmission of spike trains is rarely faithful because neurons actively transform their inputs into novel outputs. When spikes reach a synapse at high frequency, the likelihood is increased that they will generate spikes in the postsynaptic neuron, whereas at low frequency they are less effective. This type of synaptic summation acts as a temporal filter, and appears to be a general mechanism because it is found at synapses in a variety of brain structures (Chadderton, Margrie, & Hausser, 2004; Henze, Wittner, & Buzsaki, 2002; Swadlow & Gusev, 2001).

Among such synapses, a prime example is the one made by ganglion cell axons onto relay cells of the lateral geniculate nucleus (LGN), the thalamic nucleus that gates most visual signals sent from retina to cortex. It is well known that the LGN transmits only about half of all retinal spikes to the cortex (Alitto & Usrey, 2005; Cleland, Dubin, & Levick, 1971; Kaplan, Purpura, & Shapley, 1987; Lee, Virsu, & Creutzfeldt, 1983; Sincich, Adams, Economides, & Horton, 2007; Usrey, Reppas, & Reid, 1998; Weyand, 2007), yet the precise rules of this selectivity are not understood.

In particular, it is not known whether control of retinal spike transmission depends on presynaptic mechanisms such as short-term activity-dependent plasticity or postsynaptic mechanisms such as summation of synaptic potentials. Plasticity is nearly ubiquitous at synapses in the central nervous system (Zucker & Regehr, 2002), and has been demonstrated at the retinogeniculate synapse *in vitro* (Alexander & Godwin, 2005; Blitz & Regehr, 2003; Chen, Blitz, & Regehr, 2002) . However, the impact of plasticity appears to be quite minimal

in intracellular recordings obtained *in vivo* (Eysel, 1976). Thus the role of synaptic plasticity versus summation in the editing of retinal spike trains is not clear.

To examine the mechanism underlying selectivity at the retinogeniculate synapse, we recorded simultaneously the spike trains of monosynaptically connected pairs of retinal ganglion cells and LGN neurons. Although several retinal ganglion cells are likely to converge onto each LGN neuron, potentially complicating an analysis of the input-output properties, it is generally agreed that a single ganglion cell provides the dominant input to the receptive field center (Bishop, Burke, & Davis, 1958; Cleland et al., 1971; Kaplan et al., 1987; Kaplan & Shapley, 1984; Lee et al., 1983; Mastronarde, 1987a; 1987b; Sincich et al., 2007; Usrey et al., 1998; Usrey, Reppas, & Reid, 1999; Wang, Cleland, & Burke, 1985). We therefore stimulated the receptive field center with a spot of light while keeping the surround in darkness. This stimulus minimizes, but does not eliminate, the impact of corticogeniculate feedback, as the visual cortex responds best to oriented stimuli. Such recordings allowed us to derive a model of spike transmission at a single synapse *in vivo* that captures the transformation operated by a neuron onto the spike train of its main driver.

Methods

Experiments were conducted in 6 adult macaques using procedures approved by the UCSF Institutional Animal Care and Use Committee, and in accordance with NIH guidelines. Animals were anesthetized and prepared for physiological recordings as described in a recent study of the same data set (Sincich et al., 2007). The cells were selected from that study based on the duration of the records, to allow statistically meaningful analyses. Extracellular potentials recorded by single tungsten electrodes (Frederick Haer & Co., Bowdoin ME) were amplified 1000×, bandpass filtered between 300 Hz and 3kHz, and digitized at 25 kHz (Power 1401, Cambridge Electronic Design, Cambridge). Only LGN neurons with EPSPs that exhibited an absolute refractory period were included in the data set. Visual stimuli were restricted to the receptive field center, as established by manually mapping the field boundaries. The light intensity of an LED illuminating only the field center varied continuously, with a naturalistic temporal frequency power spectrum between 0.2 and 80 Hz (van Hateren, 1997). In these naturalistic stimuli, the power decreases approximately with the inverse of frequency. To assess responses to repeated trials, each 10 s stimulus included first a 5 s segment that was common across trials, and then a 5 s segment that was unique to the trial. We typically recorded more than 100 trials for each cell.

The model is defined as follows. The membrane potential is the sum of stereotyped events:

$$V(t)=\sum_j V_{syn}(t-t_j)+\sum_k V_{spike}(t-t_k)+n(t),$$

where V_{syn} is the postsynaptic potential (Figure 3**a**), V_{spike} is the waveform that includes a spike and the subsequent after-hyperpolarization (Figure 3**b**), the $\{t_j\}$ are the measured times of arrival of the retinal inputs, the $\{t_k\}$ are the times of spikes generated by the model LGN neuron, and n(t) is Gaussian-distributed white noise, initially set to zero. The model neuron spikes whenever the potential exceeds the spike threshold, $V(t) > V_{thresh}$.

The postsynaptic potential is described by a α-function:

$$V_{syn}(t)=V_{EPSP}t/\tau_{EPSP}\exp(1-t/\tau_{EPSP}),$$

where V_{EPSP} is the maximal amplitude of the EPSP, and τ_{EPSP} is the time to peak of the EPSP (which also governs its decay time). In all of our fits, we obtained $V_{EPSP} < 1$, indicating that a single isolated EPSP was never able to elicit a spike. We describe a synaptic event as pure EPSP for simplicity, but in the reality their waveforms are likely to arise from a stereotyped sequence of EPSP-IPSP, with the IPSP being provided by feedforward inhibition.

The spike waveform is described by:

$$V_{spike}(t)=\delta(t) - V_{reset} \exp(-t/\tau_{reset}),$$

where $\delta(t)$ is Dirac's delta function, V_{reset} is the magnitude of the after-hyperpolarization, and τ_{reset} is the time constant of recovery from this hyperpolarization. Events are causal, so $V_{syn}(t) = 0$ and $V_{reset}(t) = 0$ for $t<0$. In summary, the model operates on the train of afferent inputs $\{t_j\}$, and is described by 4 parameters: V_{EPSP}, τ_{EPSP}, V_{reset}, τ_{reset}.

The optimal values for the free parameters were computed as follows: (1) The spike train in each trial was Gaussian low-pass filtered ($\sigma = 5$ ms) to obtain a measure of instantaneous firing rate. (2) We obtained the best set of 4 parameters for each trial, by minimizing the sum of squared differences between model prediction and instantaneous firing rate. The parameter estimates did not change appreciably from trial to trial (Figure S3 in Supplementary Materials). (3) We fixed τ_{reset} to the median value obtained in step 2, and recomputed the best values for the 3 remaining parameters for each trial. (4) We next fixed V_{EPSP} to the median value obtained in step 3, and recomputed the best values for the 2 remaining parameters for each trial. (5) We then fixed τ_{EPSP} to the median value obtained in step 4, and recomputed the best values for V_{reset} for each trial, from which we computed the median value for V_{reset}. This procedure yielded a set of 4 parameters for each cell (Table 1). We verified that changing each parameter from its designated value yielded inferior fits (Figure S3 in Supplementary Materials).

The optimal noise level for each cell was obtained by simulating the model responses at a number of amplitudes for the noise term n(t), and finding the noise level that yielded the best fits (least mean square error) to the diagrams plotting efficacy vs. inter-EPSP input (Figure **1a**). The values thus obtained are reported in Table 1.

The model predicts responses that would be observed with intracellular recordings. To relate these responses to extracellular recordings such as ours (Figure **1a**) we high-pass filtered the model traces with a low-cut frequency of 300 Hz, which is the one used in the recordings. The resulting traces (Figure 3**a–c**) resemble qualitatively those seen in the actual recordings (Figure **1a**).

To compute the temporal frequency responses of the recorded and modeled cells (Figure 6) we used simple deconvolution. We first took Fourier Transforms of the stimulus and of the response, to obtain functions $S(\omega)$ and $R(\omega)$ that depend on frequency w. We then estimated the optimal linear filter (Theunissen et al., 2001), which is given by $F(\omega) = S^{-1}(\omega)R(\omega) / S^{-1}(\omega)S(\omega)$. We computed $F(\omega)$ independently for each trial, and then averaged across trials. For each cell, we repeated this procedure twice, once for actual responses, and then for the model responses.

The temporal tuning curves fitted to the data points are empirical functions: sums of Gaussians that can have different widths to the left and to the right of the peak. The cutoff frequencies are defined as the frequencies below and above which the responses drop below 1/e times the peak. This corresponds to the 37% level. An analysis at the 50% level gives very similar results. An analysis at the 10% level, instead, is not always possible for the low-cut frequencies, because often the low-frequency responses did not drop below that level.

Results

We recorded extracellularly from macaque LGN to compare the spike train from a neuron with the train of synaptic inputs from the neuron's dominant retinal afferent (Figure 1**a**). In recordings with high signal-to-noise ratio, we could detect both LGN spikes and retinal inputs in the form of extracellularly-recorded EPSPs, historically called "S-potentials" (Bishop et al., 1958; Cleland et al., 1971; Hubel & Wiesel, 1961; Kaplan & Shapley, 1984; Wang et al., 1985). Nearly all spikes were preceded by a retinal input, but only half (49±14%, s.d., n=12) of retinal inputs succeeded in generating a spike. The consistent shape of LGN spikes permits the use of waveform subtraction to identify the synaptic potentials that are partially merged with a spike (Sincich et al., 2007), and therefore enables reconstruction of the complete retinal spike train, which can then be compared to the LGN spike train (Figure **1b–d**). This procedure isolated a single retinal input in 9 of 12 cells, as shown by an absolute refractory period for the EPSP (Figure S1 in Supplementary Materials).

The efficacy of retinal input depended critically on EPSP history. Failed inputs were preceded by much longer intervals of silence (59 ± 8 ms, s.e., n = 9) than successful inputs (11 ± 1 ms). For example, after a 20 ms silent period the efficacy of an EPSP was low, while the efficacy of a subsequent EPSP that followed within 30 ms was much higher (Figure 2**a**). This enhancement of efficacy by paired inputs was consistent across our sample (Figure S2 in Supplementary Materials), and resembles results obtained in the cat (Usrey et al., 1998; Weyand, 2007) .

These effects might be explained by facilitation at the retinogeniculate synapse: subsequent spikes in a train could lead to progressively larger EPSPs, increasing the likelihood of reaching threshold. To test this hypothesis, we examined whether the interval between EPSPs affects the amplitude of the excitatory postsynaptic current (EPSC). We obtained robust estimates of this amplitude from the rising slope of the extracellular potential (Henze et al., 2000; Johnston & Wu, 1995). To minimize effects from polysynaptic input and membrane nonlinearities, we measured the slope from the initial portion (between 10% and 50% height) of the synaptic potential. The estimated synaptic current remained remarkably constant (Figure 2**b–c**), regardless of the interval between the first EPSP and the second EPSP. In fact, synaptic current showed a 1–5% decrease at short EPSP intervals, indicating a slight depression, rather than facilitation. These results agree with intracellular observations made in the lateral geniculate of cats, where subsequent EPSPs appear to be remarkably invariant (Eysel, 1976), and indicate that synaptic plasticity—particularly facilitation—is unlikely to play a prominent role in retinogeniculate integration during natural vision.

We therefore sought an explanation for the difference between spike trains in retina and LGN that does not rely on synaptic plasticity. One possible mechanism is postsynaptic summation: if retinal EPSPs are prolonged and summate, then the first EPSP will help the second EPSP to reach threshold. To evaluate this idea, we constructed a model of LGN responses that incorporates three basic components. The first is a synaptic potential of fixed shape and amplitude (Figure 3**a**). The second is a spike mechanism; when membrane potential reaches threshold, this mechanism spikes and injects an after-hyperpolarization which causes a refractory period (Figure 3**b**). The third is noise accounting for the synaptic inputs that we did not control and for a noisy spike threshold. The contributions of these components add linearly. Like the neurons we recorded, the model neuron fires only when an EPSP is sufficiently close to a previous EPSP (Figure 3**c**).

The model requires only 5 parameters: duration and amplitude of the EPSP, duration and amplitude of the after-hyperpolarization, and amplitude of the noise term. We estimated these parameters by optimizing a prediction of the firing rate of the LGN neuron given the timing

of EPSPs. Parameters were well constrained and remained constant for over 800 s of stimulation (Figure S3 in Supplementary Materials), yielding a single set of parameters for each neuron.

The model provided good fits to the data, accounting for 73% of the variance in the firing rate (mean, n = 9) for repeated stimuli. LGN spike trains predicted by the model (Figure 3**d**) resembled closely the recorded ones (Figure 1**d**). The model performed equally well for parvocellular and magnocellular neurons (Table 1). Most importantly, the model captured the increased efficacy of EPSPs that occur after a short inter-EPSP interval. Following a 20 ms silent period, the modeled first EPSP has low efficacy, both for the example cell (Figure 4**a**), and for the population (Figure 4**b**; see cell by cell breakdown in Table 1).

Further support for the model comes from a cell-by-cell analysis of predicted EPSC amplitudes (Figure 5). For some cells, the model predicts EPSPs that are much larger than others. To confirm these differences in EPSP size, we went back to the extracellular traces and asked whether those cells had larger EPSCs. As in the analysis in Figure 2b,c, we estimated EPSC size from the initial slope of the synaptic potential recorded extracellularly. The data show there is a positive and significant correlation across cells between the measured EPSC and the EPSP size predicted by the model. This correlation suggests that the electrode recordings could detect genuine differences in EPSP size, and indicate that the parameters of the model are physiological.

Because our model includes only the synapse from the main retinal afferent, its success suggests that our stimulus configuration largely isolates this retinal afferent, allowing us to study the basic mechanism of retinogeniculate integration. In other words, stimulation of the receptive field alone successfully minimized the impact of the numerous additional synaptic inputs to LGN relay neurons, which include retinal afferents from the receptive field surround, inhibitory input from interneurons or the thalamic reticular nucleus, and feedback projections from cortex (Sherman & Guillery, 2003). Our model fits suggest that in our reduced stimulus configuration the role of these additional synaptic inputs is simply to reduce the efficacy of the dominant retinal afferent. Indeed, these inputs are summarized in our model by the noise term, and the noise required to fit our data was largest in the cases with low peak efficacy (Figure 4**c**).

A model that captures the transformation of spike trains from one neuron to the next in the visual system should also explain the differences in the visual responses of these neurons. Therefore the model should explain the changes in visual responses between retina and LGN, at least for stimuli in the receptive field center. To test this idea, we computed temporal frequency tuning curves for the retinal responses, for the LGN responses, and for the corresponding model responses. As expected, the temporal frequency profiles of the afferent ganglion cell and LGN neuron were fairly similar (Hamamoto, Cheng, Yoshida, Smith, & Chino, 1994; Lee et al., 1983; So & Shapley, 1981), the main difference being one of overall responsivity (Figure 6**a**). Across the population, the model correctly predicted that the main difference between retinal and LGN responses was a large reduction in responsivity (Figure 6**b**), with little or no effect on preferred frequency (Figure 6**c**) or on other measures of response tuning (Figure 6**d–e**) .

Discussion

To reveal the fundamental mechanism of retinogeniculate integration we concentrated on the transmission of the dominant retinal input to an LGN neuron, the input that serves the receptive field center. We drove this retinal input by using a spot stimulus that covered only the receptive field center. More complex stimuli, such as a large-field grating, would have activated both additional retinal afferents and corticogeniculate feedback (Alitto & Usrey, 2005; Marrocco,

McClurkin, & Young, 1982; Sherman & Guillery, 2003; Sillito, Jones, Gerstein, & West, 1994; Wang, Jones, Andolina, Salt, & Sillito, 2006). With our spot stimulus, these inputs operating at nearly spontaneous background levels, which could be captured by the noise term in our model. In most cases this noise terms was small, and the model could explain a large portion of the spike trains. Our stimulus, therefore, activated only minimally the more elaborate synaptic, cellular, and circuit mechanisms that can influence LGN transmission. A complete understanding of LGN processing, of course, would need to incorporate these mechanisms. Future researchers may find it fruitful to describe these mechanisms in terms of their effects on retinogeniculate integration, and specifically on the components of our simple model.

Our results indicate that thalamic integration of spikes from the dominant retinal input depends primarily on postsynaptic summation and on basic mechanisms of spike generation. We first measured postsynaptic potentials arising from the dominant retinal input, and found no evidence for synaptic facilitation. The synaptic depression that we observed was modest, arguably smaller than seen *in vitro* (Alexander & Godwin, 2005; Blitz & Regehr, 2003; Chen et al., 2002) but highly consistent with intracellular *in vivo* recordings made in the cat (Eysel, 1976). We therefore constructed an extremely simple model of synaptic integration, one in which EPSPs have constant size irrespective of past history. This model suffices to explain the spike train of the LGN neuron based on the spike train of the dominant retinal afferent. The model explains how roughly half of the spikes in the optic nerve are “lost in transmission” and how the other half is forwarded on to the cortex, and it captures the transformation in visual responses that is operated by the LGN at least for our simplified stimulus conditions.

Our analysis succeeds in capturing the transformation between incoming spike trains and outgoing spike trains for a neuron in the primate visual system. Prior investigators have devised integrate-and-fire models to characterize the responses of retinal ganglion cells or LGN neurons to visual stimulation (Keat, Reinagel, Reid, & Meister, 2001; Pillow, Paninski, Uzzell, Simoncelli, & Chichilnisky, 2005). Our model extends this previous work in one key respect: it operates on the spike train of the relay cell’s main afferent input, not on the visual stimulus.

The linearity of postsynaptic summation that our model implies may be surprising given the highly nonlinear operation of voltage-dependent ion channels expressed in LGN neurons (McCormick & Huguenard, 1992; Williams & Stuart, 2000). Comparisons of cellular activity *in vitro* versus *in vivo* suggest that intact circuitry is more likely to hold neurons within a relatively narrow range of membrane potentials (Steriade, 2001). In the absence of spiking, the membrane potential *in vivo* rests near −60 mV, fluctuating by only a few millivolts due to synaptic noise (Deschênes, Paradis, Roy, & Steriade, 1984; Lu, Guido, & Sherman, 1992). Under these conditions, voltage-dependent ion channels may exhibit more linear behavior. A relatively steady-state activation of these channels may then predominate, yielding a linear response to EPSPs, as seen in our data and when synaptic noise is injected *in vitro* (Wolfart, Debay, Le Masson, Destexhe, & Bal, 2005).

Furthermore, it might be surprising that our model performed well even though it is not endowed with burst mechanisms that are known to be present in LGN neurons (Sherman, 2001). The reason for this success is that only few (about 3%) of the LGN spikes in our data were part of bursts and, most importantly, even these spikes were individually driven from retinal inputs (Sincich et al., 2007). In other words, to account for our data one does not need an explicit cellular mechanism that produces bursts in LGN neurons.

Finally, an important consequence of our results is that synaptic depression appears to play a much smaller role in vivo than in vitro. Perhaps the synapse does depress, but depression is constantly engaged and therefore invisible under our stimulus conditions. Our stimulus involved hundreds of consecutive presentations of 10-s segments that mimic the temporal

statistic of viewing natural scenes (van Hateren, 1997). This stimulus causes more incoming spikes than the typical stimulus protocol in vitro, where there are long periods of silence (Alexander & Godwin, 2005; Blitz & Regehr, 2003; Chen et al., 2002). If the retina had been more silent we might have seen effects of synaptic plasticity. To test for this possibility we performed two additional analyses. First, we asked if our model could predict the efficacy of incoming spikes that follow intervals up to 150 ms, during which synaptic depression would be expected to recover (Alexander & Godwin, 2005; Blitz & Regehr, 2003; Chen et al., 2002). Contrary to the synaptic depression hypothesis, efficacy did not increase after these long silences. Furthermore, the model could predict the efficacy of these long-interval incoming spikes with high accuracy. Second, we asked whether the model's performance would improve if we endowed it with synaptic depression and recovery (Varela et al., 1997). The extended model has two more parameters, so it should provide better fits. Instead, it performed just as well as the original model: the fitting procedure consistently chose parameter values that correspond to no depression. Similar to results obtained at the geniculocortical synapse (Boudreau & Ferster, 2005), therefore, we conclude that synaptic depression at the retinogeniculate synapse is much diminished in vivo compared to measurements in vitro.

Because our model characterizes the primary transformation performed by an LGN neuron, it can be built upon to understand the effect of stimuli that are more complex and behaviorally relevant. Stimuli that invade the receptive field surround would involve antagonistic inputs from additional retinal afferents, and likely a more significant role for signals from thalamus and cortex (Wang et al., 2006). Indeed, numerous behavioral and physiological variables can affect LGN integration and transmission of retinal inputs (Mukherjee & Kaplan, 1995), including anesthesia (Li, Funke, Worgotter, & Eysel, 1999), wakefulness (Weyand, Boudreaux, & Guido, 2001), alertness (Cano, Bezdudnaya, Swadlow, & Alonso, 2006), attention (O'Connor, Fukui, Pinsk, & Kastner, 2002) and binocular rivalry (Haynes, Deichmann, & Rees, 2005; Wunderlich, Schneider, & Kastner, 2005). We suggest that our model provides a foundation upon which to describe and understand the effects of these numerous factors, thus helping to clarify their underlying biophysical mechanisms and computational roles.

Supplementary Material

Refer to Web version on PubMed Central for supplementary material.

Acknowledgments

We thank Daniel Adams, John Economides, and Amar Marathe for help with experiments, Massimo Scanziani for insightful comments, and Jose-Manuel Alonso for suggesting the analysis in Figure 4c. Supported by grants NEI R01-EY10217 to JCH, and NEI R01-EY017396 to MC. The California National Primate Research Center, supported by NIH Base Grant RR00169, supplied the animals.

References

Alexander GM, Godwin DW. Presynaptic inhibition of corticothalamic feedback by metabotropic glutamate receptors. J Neurophysiol 2005;94(1):163–175. [PubMed]. [PubMed: 15772234]

Alitto HJ, Usrey WM. Dynamic properties of thalamic neurons for vision. Prog Brain Res 2005;149:83–90. [PubMed]. [PubMed: 16226578]

Bishop PO, Burke W, Davis R. Synapse discharge by single fibre in mammalian visual system. Nature 1958;182(4637):728–730. [PubMed]. [PubMed: 13590093]

Blitz DM, Regehr WG. Retinogeniculate synaptic properties controlling spike number and timing in relay neurons. J Neurophysiol 2003;90(4):2438–2450. [PubMed]. [PubMed: 14534270]

Boudreau CE, Ferster D. Short-term depression in thalamocortical synapses of the cat primary visual cortex. J Neurosci 2005;25:7179–7190. [PubMed]. [PubMed: 16079400]

Cano M, Bezdudnaya T, Swadlow HA, Alonso JM. Brain state and contrast sensitivity in the awake visual thalamus. Nat Neurosci 2006;9(10):1240–1242. [PubMed]. [PubMed: 16964255]

Chadderton P, Margrie TW, Hausser M. Integration of quanta in cerebellar granule cells during sensory processing. Nature 2004;428(6985):856–860. [PubMed]. [PubMed: 15103377]

Chen C, Blitz DM, Regehr WG. Contributions of receptor desensitization and saturation to plasticity at the retinogeniculate synapse. Neuron 2002;33(5):779–788. [PubMed]. [PubMed: 11879654]

Cleland BG, Dubin MW, Levick WR. Simultaneous recording of input and output of lateral geniculate neurones. Nat New Biol 1971;231(23):191–192. [PubMed]. [PubMed: 4325715]

Deschênes M, Paradis M, Roy JP, Steriade M. Electrophysiology of neurons of lateral thalmic nuclei in cat: resulting properties and burst discharges. J. Neurophysiol 1984;51:1196–1219. [PubMed]. [PubMed: 6737028]

Eysel UT. Quantitative studies of intracellular postsynaptic potentials in the lateral geniculate nucleus of the cat with respect to optic tract stimulus response latencies. Exp Brain Res 1976;25:469–486. [PubMed]. [PubMed: 182514]

Hamamoto J, Cheng H, Yoshida K, Smith EL 3rd, Chino YM. Transfer characteristics of lateral geniculate nucleus X-neurons in the cat: effects of temporal frequency. Exp Brain Res 1994;98(2):191–199. [PubMed]. [PubMed: 8050506]

Haynes JD, Deichmann R, Rees G. Eye-specific effects of binocular rivalry in the human lateral geniculate nucleus. Nature 2005;438(7067):496–499. [PubMed]. [PubMed: 16244649]

Henze DA, Borhegyi Z, Csicsvari J, Mamiya A, Harris KD, Buzsaki G. Intracellular features predicted by extracellular recordings in the hippocampus in vivo. J Neurophysiol 2000;84(1):390–400. [PubMed]. [PubMed: 10899213]

Henze DA, Wittner L, Buzsaki G. Single granule cells reliably discharge targets in the hippocampal CA3 network in vivo. Nat Neurosci 2002;5(8):790–795. [PubMed]. [PubMed: 12118256]

Hubel D, Wiesel TN. Integrative action in the cat's lateral geniculate body. J. Physiol. (Lond.) 1961;155:385–398. [PubMed]. [PubMed: 13716436]

Johnston, D.; Wu, SM-S. Foundations of cellular neurophysiology. Cambridge, MA: MIT Press; 1995.

Kaplan E, Purpura K, Shapley R. Contrast affects the transmission of visual information through the mammalian lateral geniculate nucleus. J. Physiol. (London) 1987;391:267–288. [PubMed: 2832591]

Kaplan E, Shapley R. The origin of the S (slow) potential in the mammalian lateral geniculate nucleus. Exp Brain Res 1984;55(1):111–116. [PubMed: 6086369]

Keat J, Reinagel P, Reid RC, Meister M. Predicting every spike. A model for the responses of visual neurons. Neuron 2001;30(3):803–817. [PubMed: 11430813]

Lee BB, Virsu V, Creutzfeldt OD. Linear signal transmission from prepotentials to cells in the macaque lateral geniculate nucleus. Exp Brain Res 1983;52(1):50–56. [PubMed: 6313418]

Li B, Funke K, Worgotter F, Eysel UT. Correlated variations in EEG pattern and visual responsiveness of cat lateral geniculate relay cells. J Physiol 1999;514(Pt 3):857–874. [PubMed: 9882756]

Lu SM, Guido W, Sherman SM. Effects of membrane voltage on receptive field properties of lateral geniculate neurons in the cat: contributions of the low-threshold Ca2+ conductance. J Neurophysiol 1992;68(6):2185–2198. [PubMed: 1337104]

Marrocco RT, McClurkin JW, Young RA. Modulation of lateral geniculate nucleus cell responsiveness by visual activation of the corticogeniculate pathway. J Neurosci 1982;2(2):256–263. [PubMed: 7062107]

Mastronarde D. Two classes of single-input X-cells in cat lateral geniculate nucleus. I. Receptive-field properties and classification of cells. J. Neurophysiol 1987;57:357–380. [PubMed]. [PubMed: 3559684]

Mastronarde DN. Two classes of single-input X-cells in cat lateral geniculate nucleus. II. Retinal inputs and the generation of receptive-field properties. J. Neurophysiol 1987;57:381–413. [PubMed]. [PubMed: 3559685]

McCormick DA, Huguenard JR. A model of the electrophysiological properties of thalamocortical relay neurons. J. Neurophysiol 1992;68:1384–1400. [PubMed: 1331356]

Mukherjee P, Kaplan E. Dynamics of neurons in the cat lateral geniculate nucleus: in vivo electrophysiology and computational modeling. J Neurophysiol 1995;74(3):1222–1243. [PubMed: 7500146]

O'Connor DH, Fukui MM, Pinsk MA, Kastner S. Attention modulates responses in the human lateral geniculate nucleus. Nat Neurosci 2002;5(11):1203–1209. [PubMed: 12379861]

Pillow JW, Paninski L, Uzzell VJ, Simoncelli EP, Chichilnisky EJ. Prediction and decoding of retinal ganglion cell responses with a probabilistic spiking model. J Neurosci 2005;25(47):11003–11013. [PubMed: 16306413]

Sherman SM. Tonic and burst firing: dual modes of thalamocortical relay. Trends Neurosci 2001;24(2): 122–126. [PubMed: 11164943]

Sherman, SM.; Guillery, RW. Thalamus. In: Shepherd, GM., editor. The Synaptic Organization of the Brain. 4th ed.. New York: Oxford University Press; 2003.

Sillito AM, Jones HE, Gerstein GL, West DC. Feature-linked synchronization of thalamic relay cell firing induced by feedback from the visual cortex. Nature 1994;369(6480):479–482. [PubMed: 8202137]

Sincich LC, Adams DL, Economides JR, Horton JC. Transmission of spike trains at the retinogeniculate synapse. J Neurosci 2007;27(10):2683–2692. [PubMed: 17344406]

So YT, Shapley R. Spatial tuning of cells in and around lateral geniculate nucleus of the cat: X and Y relay cells and perigeniculate interneurons. J Neurophysiol 1981;45(1):107–120. [PubMed: 6259298]

Steriade M. Impact of network activities on neuronal properties in corticothalamic systems. J Neurophysiol 2001;86(1):1–39. [PubMed: 11431485]

Swadlow HA, Gusev AG. The impact of 'bursting' thalamic impulses at a neocortical synapse. Nat Neurosci 2001;4(4):402–408. [PubMed: 11276231]

Theunissen FE, David SV, Singh NC, Hsu A, Vinje WE, Gallant JL. Estimating spatio-temporal receptive fields of auditory and visual neurons from their responses to natural stimuli. Network 2001;12(3): 289–316. [PubMed: 11563531]

Usrey WM, Reppas JB, Reid RC. Paired-spike interactions and synaptic efficacy of retinal inputs to the thalamus. Nature 1998;395(6700):384–387. [PubMed: 9759728]

Usrey WM, Reppas JB, Reid RC. Specificity and strength of retinogeniculate connections. J Neurophysiol 1999;82(6):3527–3540. [PubMed]. [PubMed: 10601479]

van Hateren JH. Processing of natural time series of intensities by the visual system of the blowfly. Vision Res 1997;37(23):3407–3416. [PubMed]. [PubMed: 9425553]

Varela JA, Sen K, Gibson J, Fost J, Abbott LF, Nelson SB. A quantitative description of short-term plasticity at excitatory synapses in layer 2/3 of rat primary visual cortex. J. Neurosci 1997;17:7926–7940. [PubMed]. [PubMed: 9315911]

Wang C, Cleland BG, Burke W. Synaptic delay in the lateral geniculate nucleus of the cat. Brain Res 1985;343(2):236–245. [PubMed]. [PubMed: 2996696]

Wang W, Jones HE, Andolina IM, Salt TE, Sillito AM. Functional alignment of feedback effects from visual cortex to thalamus. Nat Neurosci 2006;9(10):1330–1336. [PubMed]. [PubMed: 16980966]

Weyand TG. Retinogeniculate transmission in wakefulness. J Neurophysiol 2007;98:769–785. [PubMed]. [PubMed: 17553944]

Weyand TG, Boudreaux M, Guido W. Burst and tonic response modes in thalamic neurons during sleep and wakefulness. J Neurophysiol 2001;85(3):1107–1118. [PubMed]. [PubMed: 11247981]

Williams SR, Stuart GJ. Action potential backpropagation and somato-dendritic distribution of ion channels in thalamocortical neurons. J Neurosci 2000;20(4):1307–1317. [PubMed]. [PubMed: 10662820]

Wolfart J, Debay D, Le Masson G, Destexhe A, Bal T. Synaptic background activity controls spike transfer from thalamus to cortex. Nat Neurosci 2005;8(12):1760–1767. [PubMed]. [PubMed: 16261132]

Wunderlich K, Schneider KA, Kastner S. Neural correlates of binocular rivalry in the human lateral geniculate nucleus. Nat Neurosci 2005;8(11):1595–1602. [PubMed]. [PubMed: 16234812]

Zucker RS, Regehr WG. Short-term synaptic plasticity. Annu Rev Physiol 2002;64:355–405. [PubMed]. [PubMed: 11826273]

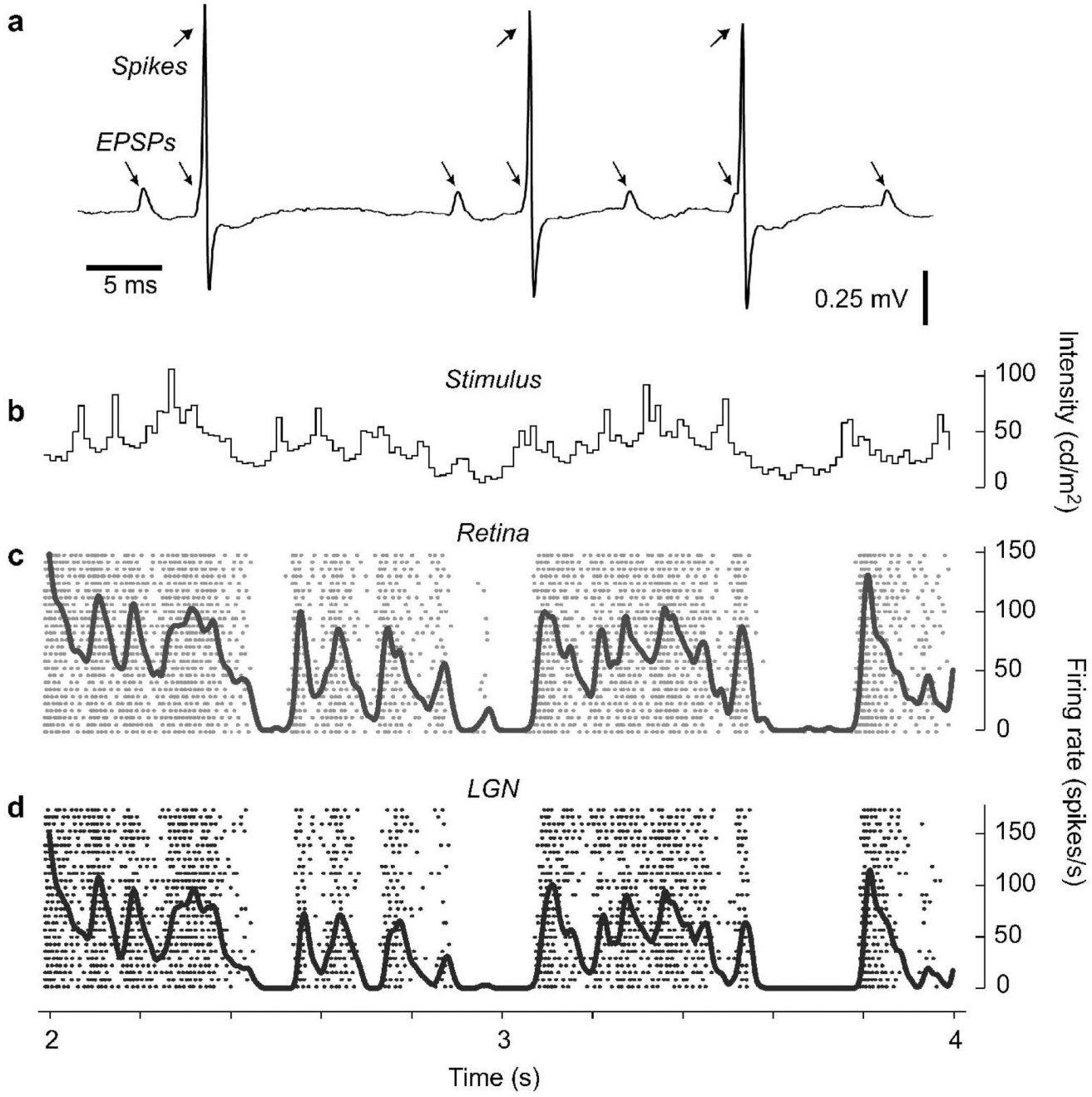

Figure 1.

Basic properties of retinal EPSPs and LGN spikes. **a**, Spikes and EPSPs recorded simultaneously with an extracellular microelectrode. **b**, A 2 sec segment of the noise stimulus, representing a naturalistic temporal frequency spectrum. **c–d**, Rasters of synaptic potentials (**c**) and LGN spikes (**d**) recorded during 25 repeats of the stimulus in **b**. Curves indicate firing rates averaged over 100 trials (right scale). Cell 121R15-5.

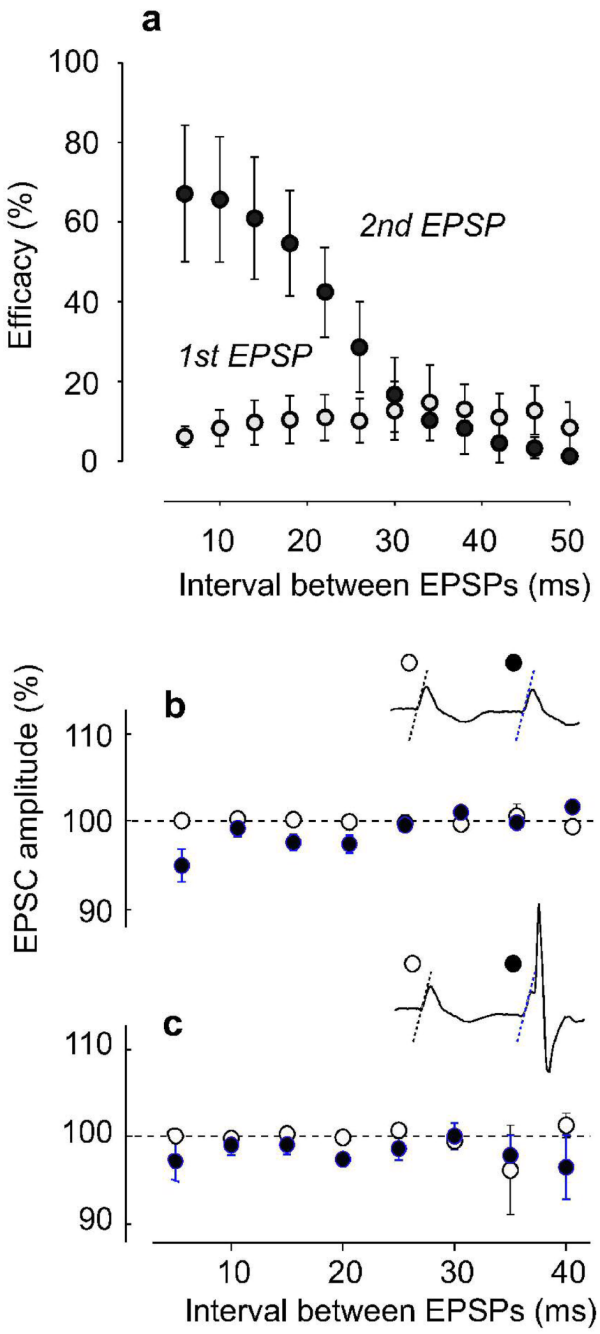

Figure 2.

Synaptic summation and plasticity statistics for the cell population. **a**, Efficacy of EPSP pairs, when the first EPSP occurred after > 20 ms silent period (average of 9 cells). The first EPSP has low efficacy (open circle), the second one has high efficacy if it follows soon thereafter (closed circle). Error bars are ± 2 s.e. **b,c**, Synaptic current (EPSC) estimated from the initial slope of the extracellularly-recorded EPSP (normalized to EPSP at the 5 ms interval). Synaptic currents showed no facilitation, regardless of whether the second EPSP failed (**b**) or succeeded (**c**) in eliciting a spike.

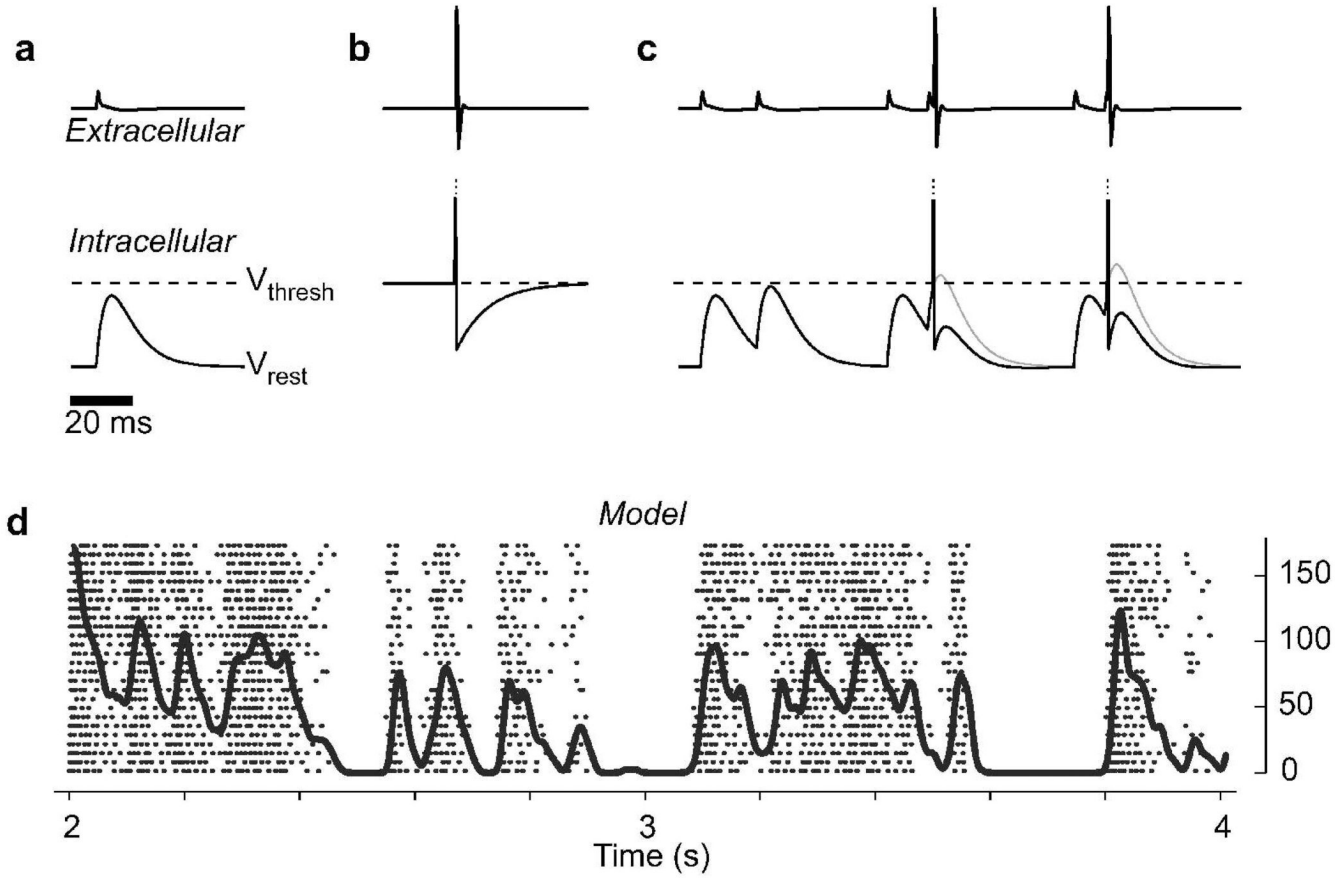

Figure 3.

Predicting retinogeniculate integration with a summation model. **a**, Model EPSP induced by a retinal spike, and corresponding extracellular trace (top). **b**, Model spike and subsequent after-hyperpolarization, and corresponding extracellular trace (top). **c**, Responses of the model to three pairs of retinal inputs, with decreasing EPSP interval. The first EPSP in the pair never reaches threshold; the second can reach threshold only if it combines with the first. **d**, Rasters and firing rates predicted by the model (cf. Figure 1**d**).

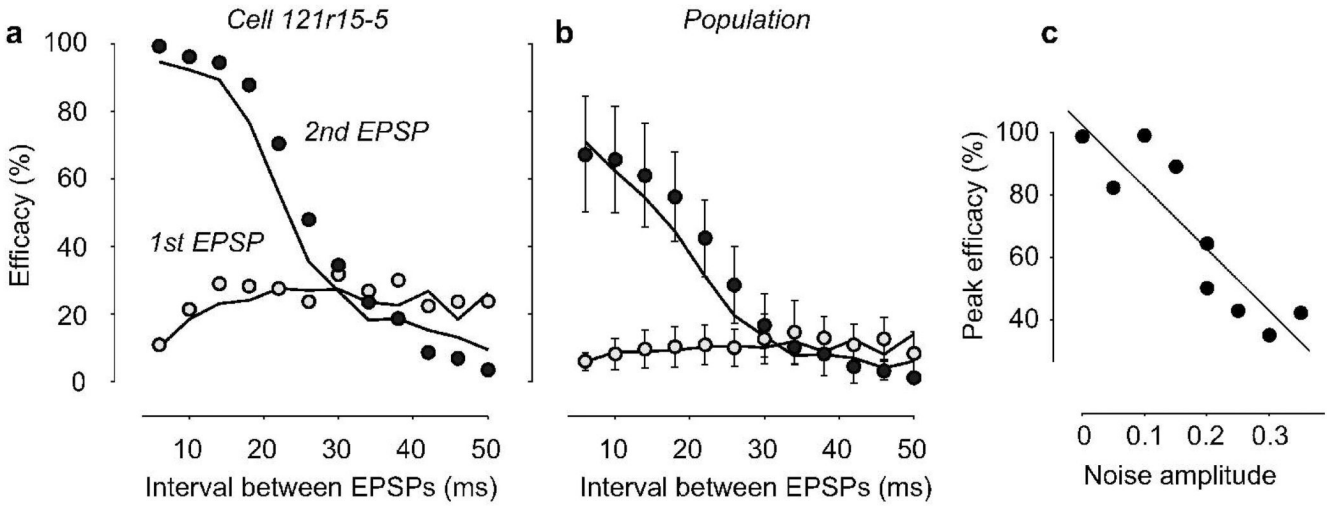

Figure 4.

Comparison of observed and predicted synaptic efficacy. **a**, Efficacy of synaptic inputs in a pair, and predictions of the model (curves). Same cell as in Figure 1. **b**, Efficacy averaged over 9 cells (same data as Figure 1**a**) along with model predictions (curves). Error bars are ± 2 s.e. (n = 9). **c**, The noise required to explain the data is negatively correlated with the synapse's peak efficacy (measured 5 ms after a prior EPSP); regression line, $r = -0.89$, $p < 0.01$. The amplitude of the noise determines the standard deviation of a Gaussian distribution. Its units are the same as those of V_{syn}, which has a value of zero at rest, and of one at threshold.

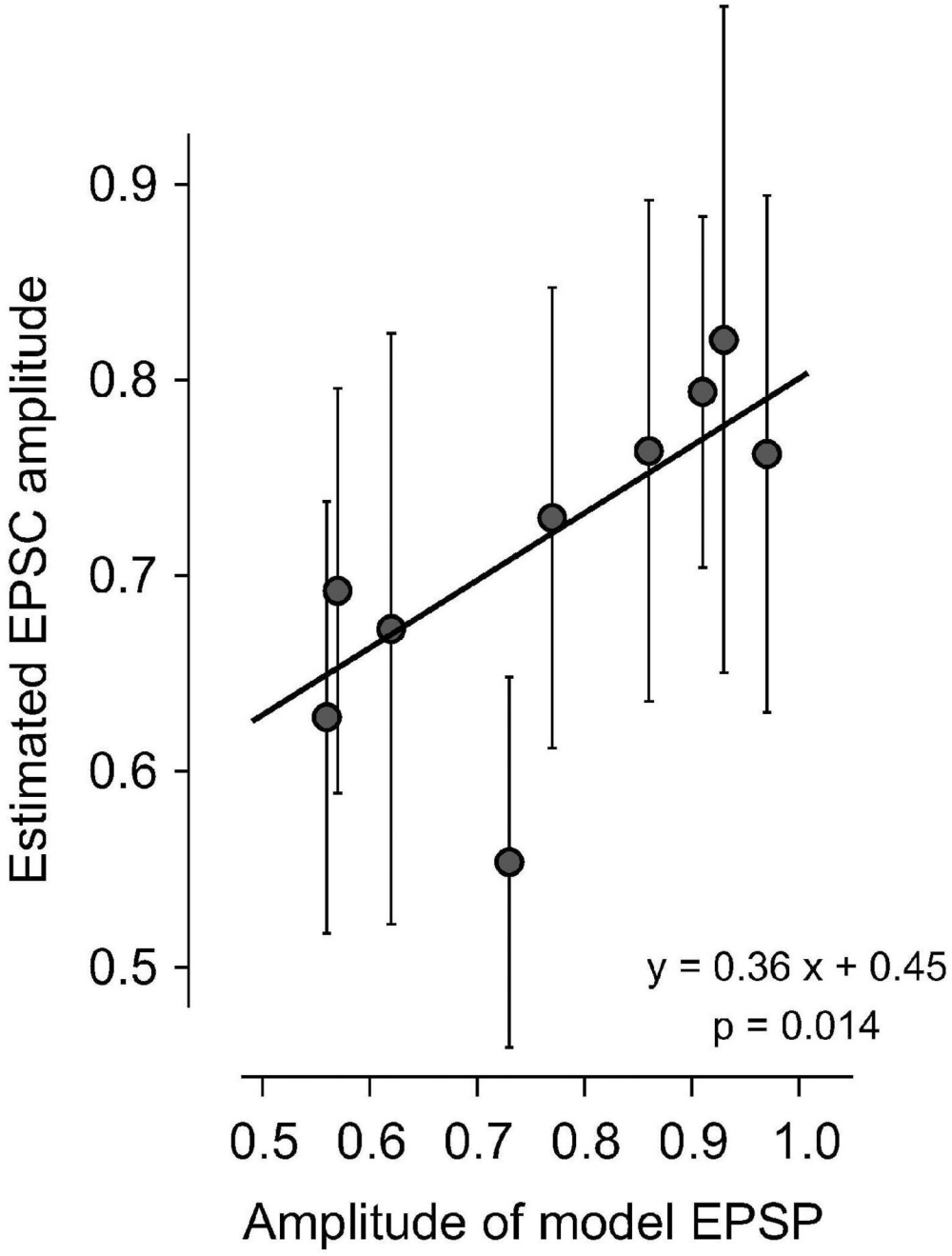

Figure 5.

Measured EPSC amplitude correlates with model predictions. The abscissa indicates the amplitude of each cell's EPSP as fitted by the model (V_{epsp}, from Table 1). The ordinate indicates the EPSC size estimated from the initial slope of the synaptic potentials measured extracellularly, which is an estimate of EPSC amplitude. To control for variations across cells in electrode impedance and distance from the soma, we corrected these measures by dividing by the amplitude of the extracellularly measured spike. Slope measurements were taken for ~4000 synaptic potentials. Error bars are ±1 s.d. The regression was performed through robust fitting, which gave a small weight to the outlier. There is a positive and significant ($p = 0.014$) correlation across cells between the measured EPSC and the EPSP size predicted by the model.

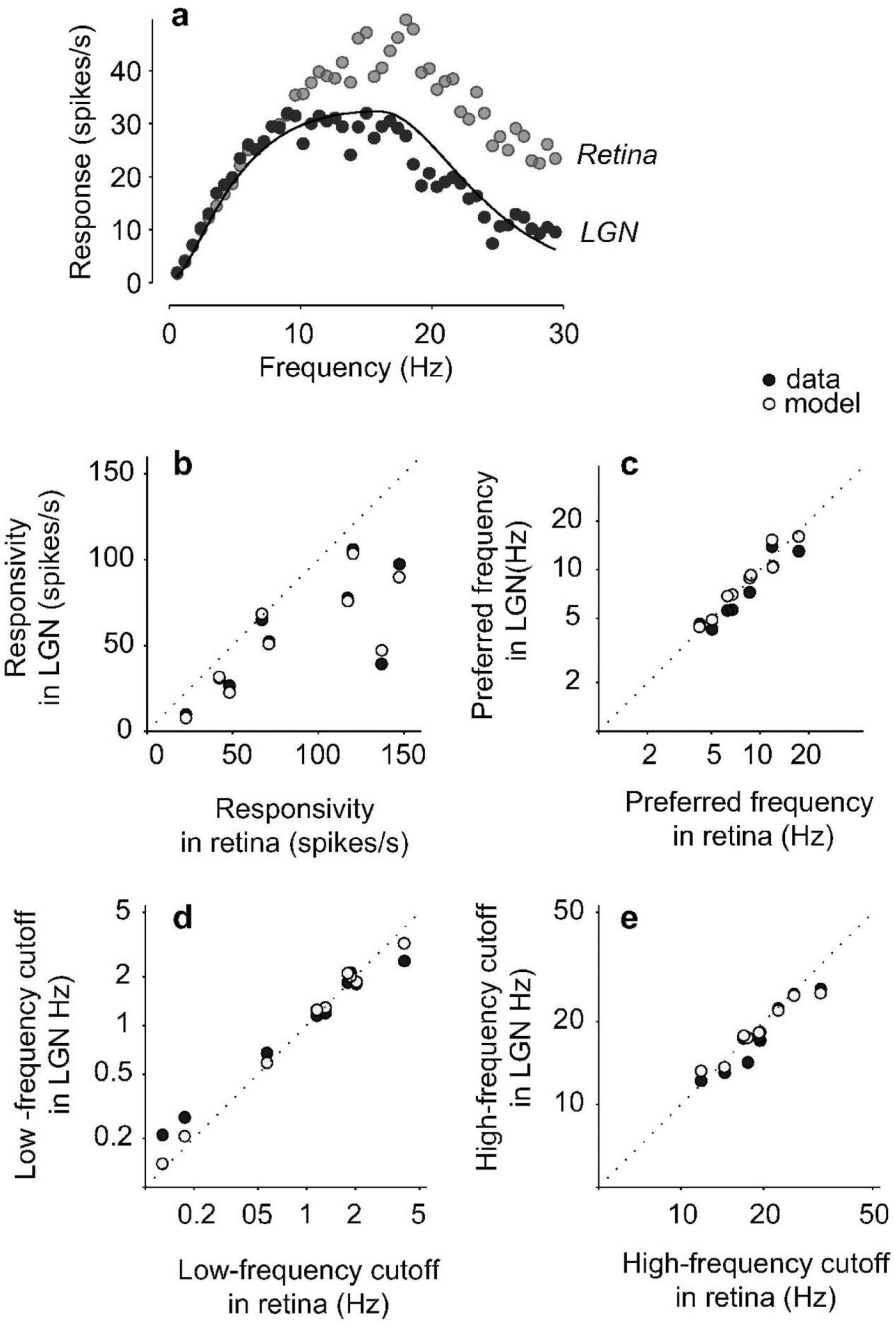

Figure 6.

Observed and predicted response properties of LGN neurons. **a**, Temporal frequency tuning curves for synaptic potentials (gray), LGN spikes (black), and modeled responses (curve). Cell 121R14-4. **b**: Responsivity of retinal inputs (abscissa) and LGN outputs (ordinate) for 9 LGN neurons (closed circles) and corresponding model predictions (open circles). **c–e**, Same for the preferred temporal frequency (**c**), for the low-frequency cutoff (**d**), and for the high-frequency cutoff (**e**).

Table 1

Fit quality, fit parameters, and basic information about the 9 cells in the analyzed sample. No clear parameter differences were seen between magnocellular and parvocellular neurons or between ON-center and OFF-center neurons.

Unit	% variance	τ_{EPSP} (ms)	V_{EPSP}	τ_{reset} (ms)	V_{reset}	V_{noise}	ON/OFF	P/M
120L15-1	71.0	7.4	0.77	6.3	4.39	0.15	ON	P
121R11-1	75.0	14.2	0.86	20.9	2.37	0.35	ON	--
121R13-4	42.5	8.4	0.62	9.5	6.64	0.30	ON	M
121R14-4	46.7	17.2	0.57	33.4	0.78	0.00	ON	--
121R15-5	85.9	5.8	0.93	7.5	1.34	0.10	ON	P
121R7-1	92.4	5.8	0.97	6.3	2.54	0.05	ON	M
122R4-2	74.0	6.3	0.91	29.9	0.85	0.20	OFF	P
122R4-3	87.3	5.6	0.73	12.3	1.04	0.20	OFF	M
122R4-5	78.7	6.0	0.56	12.0	0.82	0.25	ON	M
Mean	72.6	8.5	0.77	15.4	2.31	0.18		

J Vis. Author manuscript; available in PMC 2010 July 12.